Thermodynamic and kinetic properties of NH_3-K_2CO_3-CO_2-H_2O system for carbon capture applications

Lillia, Stefano; Bonalumi, Davide; Fosbøl, Philip L.; Thomsen, Kaj; Jayaweera, Indira; Valenti, Gianluca

Published in:
International Journal of Greenhouse Gas Control

Link to article, DOI:
10.1016/j.ijggc.2019.03.019

Publication date:
2019

Document Version
Peer reviewed version

Thermodynamic and kinetic properties of NH_3-K_2CO_3-CO_2-H_2O system for carbon capture applications

Stefano Lillia[a], Davide Bonalumi[a1], Philip L. Fosbøl[b], Kaj Thomsen[b], Indira Jayaweera[c] and Gianluca Valenti[a]

[a]*Politecnico di Milano – Dipartimento di Energia, Via R. Lambruschini 4, Milano, Italy*
[b]*Technical University of Denmark, Department of Chemical Engineering, Center for Energy Resource Engineering, Søltofts Plads, 2800, Kgs. Lyngby, Denmark*
[c]*SRI International, 333 Ravenswood Avenue, Menlo Park, CA 94025, USA*

Keywords:

- CO_2 capture
- Kinetics
- Rate of absorption
- Ammonia
- Mixed-Salt Technology
- Experimental measurements

Highlights:

- K_2CO_3 addition reduced the heat of CO_2 desorption with respect to aqueous NH_3 solvent
- Higher desorption temperature reduced the heat of desorption
- Upon addition of K_2CO_3, the NH_3 partial pressure of the solvent decreased
- K_2CO_3 addition reduced the rate of CO_2 absorption compared to that in aqueous NH_3
- Free NH_3 molality was correlated with the CO_2 absorption rate

Abstract

An innovative solvent based on the quaternary system CO_2-NH_3-K_2CO_3-H_2O is reported and characterized in terms of its thermodynamic properties and rate of CO_2 absorption. Thermodynamic properties of the solvent such as vapor-liquid equilibrium, solid-liquid equilibrium, and the heat of desorption were modelled with the Extended UNIQUAC thermodynamic model. The kinetics of CO_2 absorption in the solvent were studied experimentally with a wetted wall column set-up. The absorption

rate was investigated with respect to temperature, ammonia concentration, potassium carbonate concentration, and CO_2 loading, under the typical operating conditions of a capture plant. Globally, the solvent has a number of interesting properties for CO_2 capture applications. Indeed, adding K_2CO_3 to the ammonia solvent reduced both the ammonia slip and the heat of desorption. Experimental analysis showed that the kinetics of absorption were mainly influenced by the reaction between free ammonia and CO_2. Hence, the overall mass transfer coefficient decreased when increasing the K_2CO_3 content of the solvent.

1. Introduction

The correlation between anthropogenic carbon dioxide emissions in the atmosphere and the greenhouse effect is considered by many institutions to be a primary cause of the phenomenon of global warming. One of the most mature technologies for CO_2 capture at the emission source is the solvent-based chemical absorption/desorption process (Rochelle et al., 2011)(Rochelle, 2011). Widely known chemical sorbents for CO_2 capture include aqueous solutions of amines such as monoethanolamine (MEA), *N*-methyl-diethanolamine (MDEA), and piperazine.

Currently, mature alternatives to amine-based technologies that have been developed beyond pilot and/or validation stages include ammonia- and potassium-carbonate-based aqueous solvents. Both the ammonia and the potassium carbonate solvents have low toxicity and do not suffer from the problem of degradation, unlike the amine-based solvents. Moreover, from the perspective of life cycle analysis (LCA) (Petrescu et al., 2017)(Grant et al., 2014), CO_2 capture technologies using inorganic solvents, such as NH_3 or K_2CO_3, have a lower environmental impact with respect to the amine-based counterparts, due mainly to the production chain of the solvent itself.

Solvents based on ammonia are capable of capturing CO_2 at higher loadings compared to amine-based solvent technology (Bai and Yeh, 1997). In addition, the ammonia-based technology can strip CO_2 at

high pressure, reducing the CO_2 compression costs (Bonalumi et al., 2016). However, such technology requires cooling of the flue gas and the solvent, as well as washing of the treated gas to reduce ammonia emissions (Kong et al., 2011). In comparison to the ammonia-based solvent technology, the potassium-carbonate-based technology does not involve any issues with emissions. However, it suffers from low CO_2 absorption efficiency, very low loading capacity, and the solvent cannot be regenerated at high pressure. As such, new approaches for improved potassium-carbonate-based CO_2 capture technology have been in development for decades (Williamson and Matheus, 1924)(Mumford et al., 2012)(Gladis et al., 2017).

The aim of this work was to study the thermodynamic properties and kinetics of CO_2 absorption of mixtures of NH_3 and K_2CO_3 in the same solvent with new data. This mixture was expected to be characterized by a low heat duty of regeneration, a reduced ammonia slip in comparison to the aqueous ammonia solvent, and a high regeneration pressure, combining the best properties of the two individual solvents. The studied solvent has been termed the 'mixed-salt technology solvent' in a patent by SRI International, and part of its characterization has already been published (Jayaweera et al., 2014)(Jayaweera et al., 2016)(Jayaweera et al., 2017). In these previous investigations, the background of the process was studied, and the results confirmed some of the promising properties of the solvent such as the reduced ammonia slip and heat of CO_2 desorption, both of which will be described in further detail in the present work. Moreover, the cited works reported some performance features that can be expected from the use of this solvent in a carbon capture process.

Modelling of the thermodynamic properties of the solvent was performed with the Extended UNIQUAC thermodynamic model (Thomsen and Rasmussen, 1999). The model parameters were determined on the basis of experimental data for the ternary systems NH_3-CO_2-H_2O, K_2CO_3-CO_2-H_2O, and K_2CO_3-NH_3-H_2O, which was updated in a 2018 report by SRI International (Jayaweera and Jayaweera, 2018).

The kinetics of CO_2 absorption in the solvent were investigated through an experimental study of the absorption reaction of CO_2 in the K_2CO_3-NH_3-H_2O system. This study was conducted with a wetted wall column set-up (Darde et al. 2011). Experiments were designed in order to determine the absorption rate with respect to temperature, ammonia concentration, potassium carbonate concentration, and CO_2 loading, under typical operating conditions of a capture plant. Next, the overall mass transfer coefficient was analyzed, and the kinetics of CO_2 absorption were described with the support of the thermodynamic model used for calculating the speciation in the bulk liquid. The result is the description of the solvent and the evidence of the advantages and disadvantages for its utilization for carbon capture applications. The following sections describe: (i) the thermodynamic model and its validation with data from the literature; (ii) the experimental set-up used for the measurement of the rate of absorption; iii) and finally the thermodynamic properties and the kinetic characteristics of absorption of the mixed-salt technology solvent.

2. Extended UNIQUAC thermodynamic model

The thermodynamic properties of the solvent were assessed with the Extended UNIQUAC thermodynamic model (Thomsen and Rasmussen, 1999). The current model used contains a further recalibration of the parameters of the original version of 1999 (Jayaweera and Jayaweera, 2018). The model parameters were determined on the basis of experimental data taken over the temperature range from the freezing point of the solutions up to 200 °C. The parameters for the NH_3-CO_2-H_2O system, the K_2CO_3-CO_2-H_2O system, and the K_2CO_3-NH_3-H_2O system were determined based on more than 8000 experimental data points recorded at pressures of up to 100 bar.

The reactions considered for the equilibrium and implemented in the thermodynamic model in order to determine the speciation and ion concentration in the liquid phase are shown as reactions R1–R5.

$$H_2O \leftrightarrow H^+ + OH^- \quad \text{(R1)}$$

$$NH_3 + H_2O \leftrightarrow NH_4^+ + OH^- \quad \text{(R2)}$$

$$HCO_3^- \leftrightarrow CO_3^{--} + H^+ \quad \text{(R3)}$$

$$CO_2 + H_2O \leftrightarrow HCO_3^+ + H^+ \quad \text{(R4)}$$

$$NH_3 + HCO_3^- \leftrightarrow NH_2COO^- + H_2O \quad \text{(R5)}$$

97

98 In addition, the solubilities of the salts KOH, KOH·H_2O, KOH·$2H_2O$, K_2CO_3, $2K_2CO_3 \cdot 3H_2O$,
99 $K_2CO_3 \cdot 6H_2O$, $KHCO_3$, $2K_2CO_3 \cdot 4KHCO_3 \cdot 3H_2O$, $(NH_4)_2CO_3 \cdot K_2CO_3$, $(NH_4)_2CO_3$, $(NH_4)_2CO_3 \cdot H_2O$,
100 NH_4HCO_3, $(NH_4)_2CO_3 \cdot 2(NH_4HCO_3)$, NH_2COONH_4, and that of ice were considered. For the gas phase,
101 the Soave-Redlich-Kwong equation of state was used as the model, without any additional parameters.
102 Figure 1to Figure 3 depict the agreement between the thermodynamic model and experimental data.
103 Other comparisons between the model and experimental data used for model validation have been
104 reported in previous works (Darde et al., 2012)(Jayaweera and Jayaweera, 2018).

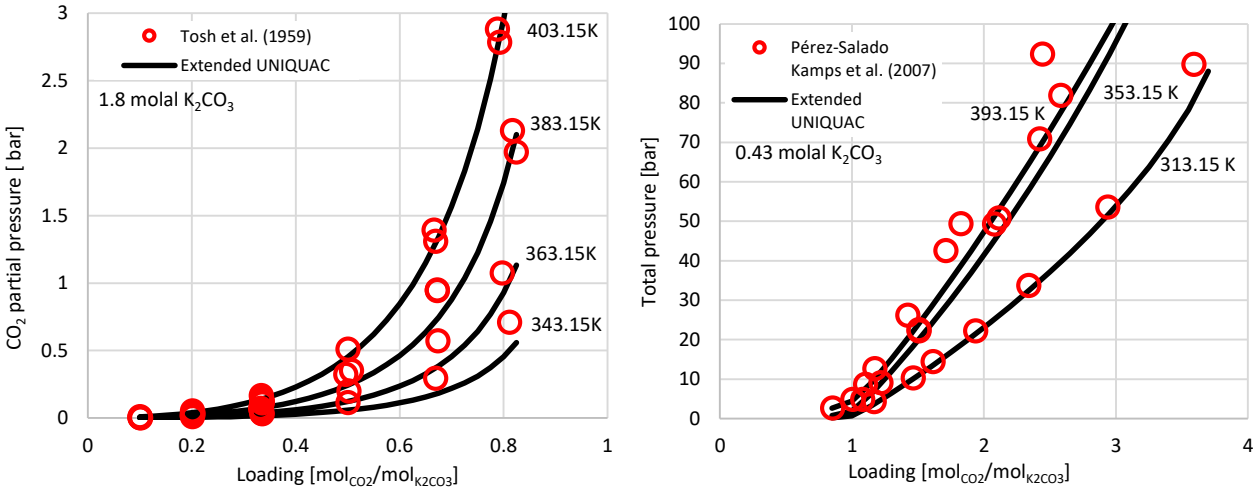

105

106 Figure 1. (Left) CO_2 partial pressure over aqueous solutions of 1.8 molal K_2CO_3 loaded with CO_2. Model
107 calculations are in good agreement with experimental data from Tosh et al. (1959); (right) total pressure
108 over aqueous solutions of 0.43 molal K_2CO_3 with high loadings of CO_2. Model calculations are in good
109 agreement with experimental data from Kamps et al. (2007).

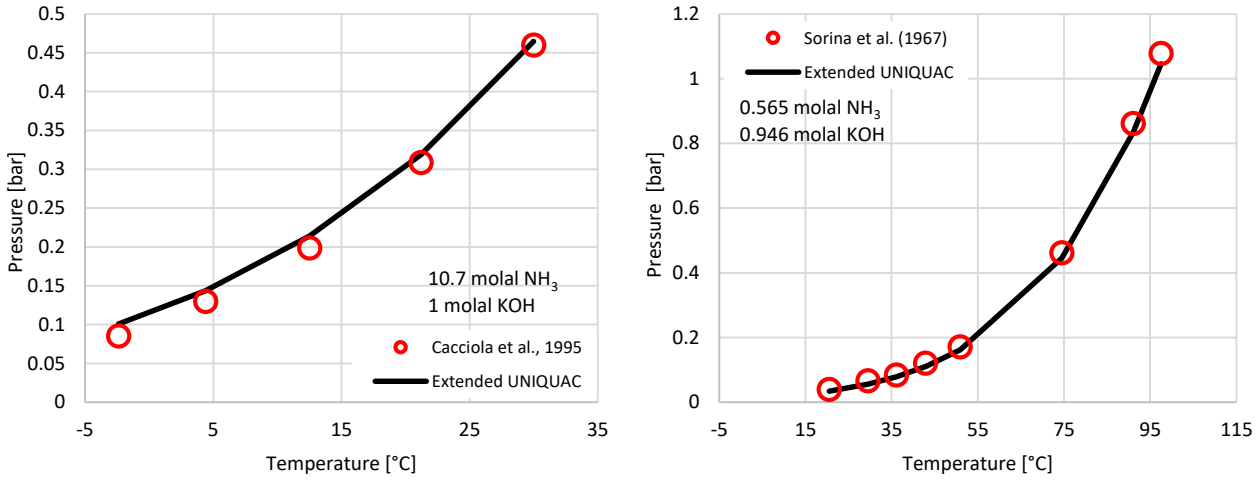

Figure 2. Bubble pressure above KOH solutions with different amounts of ammonia as a function of temperature (Cacciola et al., 1995)(Sorina et al., 1967).

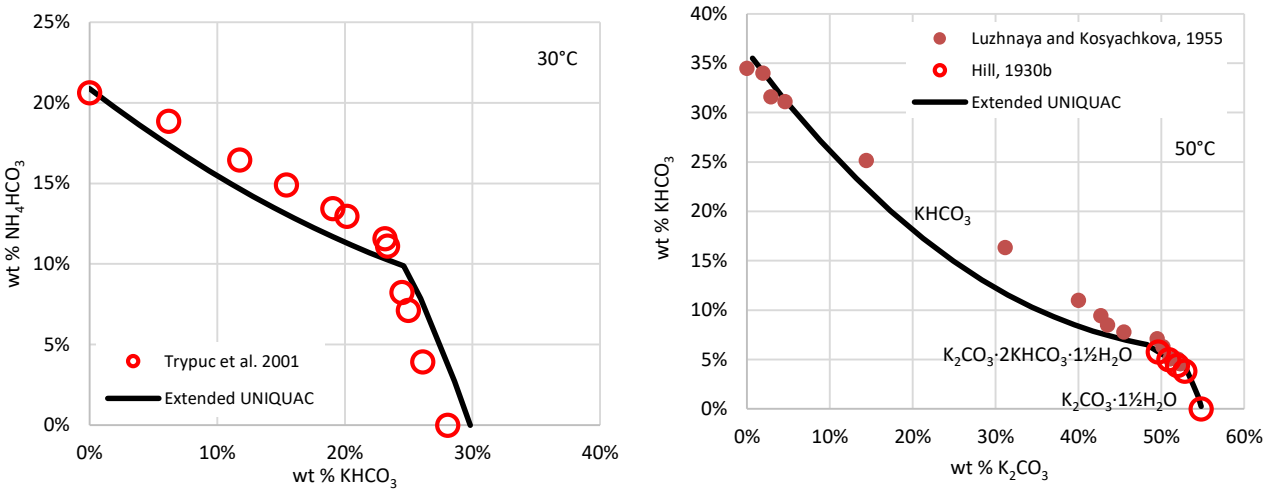

Figure 3. (Left) Solubility in the ternary $KHCO_3$-NH_4HCO_3-H_2O system at 30 °C (Trypuć and Kiełkowska, 1996); (right) solubility in the K_2CO_3-$KHCO_3$-H_2O system at 50 °C (Luzhnaya and Kosyachkova, 1955)(Hill, 1930).

3. Measurement of the absorption rate with the wetted wall column.

In this study, the wetted wall column set-up (WWC) was applied for the measurement of the CO_2 absorption rate (Darde et al., 2011). The WWC reproduces the mass transfer conditions of a packed column on a smaller scale. The experimental analysis allows comprehension of the overall phenomenon,

and thereby recognition of which of the operational parameters influence the CO_2 absorption to a greater degree. The methodology applied for the measurement of the overall mass transfer coefficient is explained in the work by Lillia et al. (2018a). The following section first reports a brief description of the experimental set-up, followed by a description of the approach used for the measurement of the overall mass transfer coefficient.

3.1. Experimental set-up description

Figure 4 shows a sketch of the WWC experimental set-up. The system was equipped with the necessary mass flow controllers, valves, temperature controllers, and detectors for measuring the CO_2 composition of the inlet gas mixture in the chamber. A bypass valve in the gas line before the reaction chamber allowed the measurement of CO_2 concentration before and after the absorption reactions, sending the flow straight to the CO_2 probe or to the reaction chamber.

The thermostatic bath controlled the temperature of the reaction by heating the gas, the solvent, and the reaction chamber to predetermined temperatures. The solvent was prepared with a known composition of NH_3, K_2CO_3, and CO_2 loading, and pumped into the reaction chamber which was comprised of a glass cylinder with a stainless steel tube inside. During the measurement, the solvent flows from inside the stainless steel tube and falls down around its external surface in a thin film, which permits simple measurement of the contact area between the liquid and the gas phase.

The aim of the experiment was to assess the relation between the CO_2 flux absorbed by the solvent and the CO_2 concentration in the gas mixture at a given temperature, by measuring the contact area between the gas and the liquid and the amount of CO_2 absorbed in the chamber. The methodology used for solvent preparation and the experimental procedure were reported previously (Lillia et al., 2018b), while the description of the overall mass transfer coefficient measurement is presented in the following section.

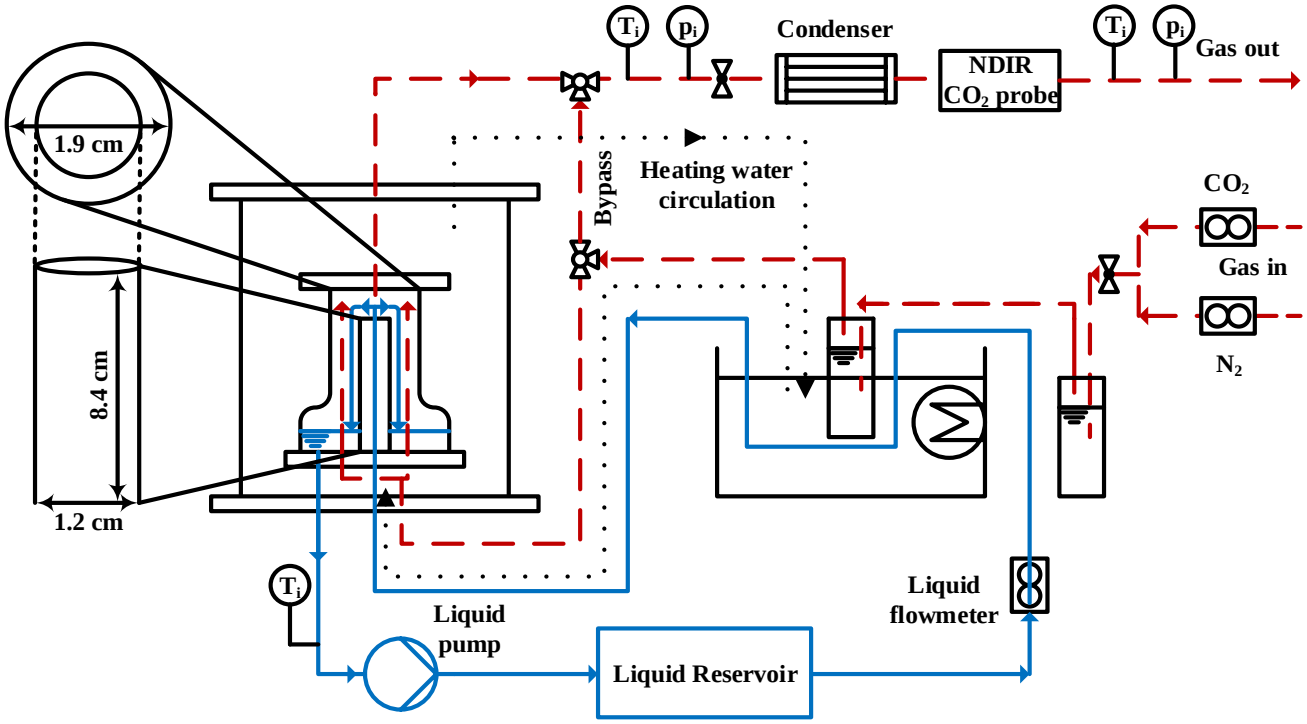

Figure 4. Wetted wall column (WWC) layout: the solid blue line represents the solvent; the dashed red line represents the gas mixture; and the dotted black line represents the cooling water from the thermostatic bath (Gladis et al., 2017).

3.2. Overall mass transfer constant measurement

The gas flow fed to the reactor was composed of N_2, CO_2, and H_2O. The WWC set-up measured the CO_2 concentration at the inlet and the outlet of the reactor. Moreover, the gas flow passed through two saturators at a set temperature, so the water concentration and consequently the nitrogen concentration were also known. Together, this data allowed the calculation of the flow of absorbed CO_2 (in moles), ΔN_{CO_2}[mol/s], according to:

$$\Delta N_{CO_2} = \frac{\left(N_{N_2} + N_{H_2O}\right)\left(y_{CO_2}^{bypass} - y_{CO_2}^{WWC}\right)}{\left(1 - y_{CO_2}^{bypass}\right)\left(1 - y_{CO_2}^{WWC}\right)} \quad (1)$$

where N_{N_2} [mol/s] is the flow of N_2 in moles, N_{H_2O} [mol/s] the flow of H_2O in moles, $y_{CO_2}^{bypass}$ [-] is the mole fraction in the bypass, and $y_{CO_2}^{WWC}$ [-] is the mole fraction after the reactor. The CO_2 probe measured the volumetric concentration of CO_2, and consequently the mole fraction of CO_2 could be determined. The gas-liquid interface is the surface where the CO_2 passes from the gas to the liquid phase, and allows for calculation of the surface flow of CO_2. This area was computed by measuring the contact area between the stainless steel cylinder wetted by the solvent and the gas phase. The total area was calculated as the area of the cylinder wetted by the liquid film, while the flow (in moles) specific to the gas-liquid interface, φ_{CO_2} [mol/(m^2 s)], was computed as:

$$\varphi_{CO_2} = \frac{\Delta N_{CO_2}}{A_{int}} \tag{2}$$

where A_{int} [m^2] is the surface of the gas-liquid interface and ΔN_{CO_2} [mol/s] is the carbon dioxide flow absorbed (in moles).

Considering the gas flow of an ideal mixture of ideal gases, the CO_2 partial pressure, $P_{CO_2}^{WWC}$ [Pa], in the reactor is given by:

$$P_{CO_2}^{WWC} = y_{CO_2}^{WWC} P_{TOT}^{WWC} \tag{3}$$

where P_{TOT}^{WWC} [Pa] is the total pressure inside the reactor. Since the molar fraction of CO_2 in the gas phase is not constant along the reactor, the partial pressure in the reactor, $P_{CO_2}^{gas}$ [Pa], is evaluated using the logarithmic mean:

$$P_{CO_2}^{gas} = \frac{P_{CO_2}^{in} - P_{CO_2}^{out}}{ln\left(\frac{P_{CO_2}^{in}}{P_{CO_2}^{out}}\right)} \tag{4}$$

where $P_{CO_2}^{in}$ [Pa] is the partial pressure of CO_2 in the reactor inlet and $P_{CO_2}^{out}$ [Pa] is the partial pressure of CO_2 in the reactor outlet.

According to Fick's law, the linear proportionality between the flux of carbon and the carbon dioxide concentration gradient in the direction of diffusion can be described by the diffusion coefficient.

The two-film theory is a model used to describe the absorption of CO_2 from a gas bulk with a partial pressure $P_{CO_2}^{gas}$ CO_2 [Pa] by a liquid with CO_2 concentration $C_{CO_2}^{liq}$ [mol/m^3] (Figure 5).

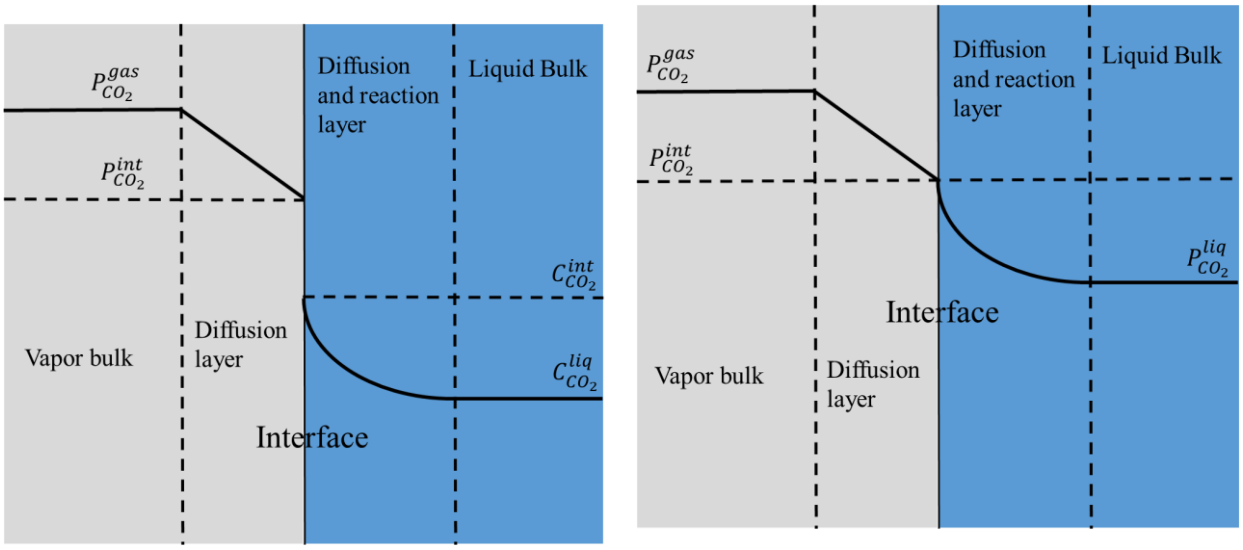

Figure 5. Left: the solid line represents the CO_2 partial pressure profile in the vapor bulk and the diffusion layer, whereas it represents the CO_2 concentration profile in the diffusion and reaction layer and the liquid bulk, according to the two-film theory (Lewis and Whitman, 1924). Right: the solid line in both the gas and liquid phases represent the CO_2 partial pressure profile according to the two-film theory (Lewis and Whitman, 1924).

In order to make the mass transfer phenomenon dependent on the partial pressure of CO_2 also in the liquid phase, the partial pressure of CO_2 in liquid phase is calculated as:

$$P_{CO_2} = H_{CO_2}\, C_{CO_2} \tag{5}$$

where H_{CO_2} [(Pa m^3)/mol] is the partition coefficient and C_{CO_2} [mol/m^3] is the CO_2 concentration in the liquid phase. In this work, the partition coefficient was taken as the Henry constant of CO_2 in the solvent.

The two-film theory (Lewis and Whitman, 1924) describes the flux of CO_2 as the product of a mass transfer coefficient and the corresponding driving force which is expressed as the difference in CO_2 partial pressure or CO_2 concentration. Within this approach, the following expressions hold true:

$$\varphi_{CO_2}^{G} = k_G\left(P_{CO_2}^{gas} - P_{CO_2}^{int}\right) \tag{6}$$

$$\varphi_{CO_2}^{L} = k_{liq}\left(C_{CO_2}^{int} - C_{CO_2}^{liq}\right) = \frac{k_{liq}}{H_{CO_2}}\left(P_{CO_2}^{int} - P_{CO_2}^{liq}\right) = k'_{liq}\left(P_{CO_2}^{int} - P_{CO_2}^{liq}\right) \tag{7}$$

$$\varphi_{CO_2} = K_{ov}\left(P_{CO_2}^{gas} - P_{CO_2}^{liq}\right) \tag{8}$$

$$\varphi_{CO_2} = \varphi_{CO_2}^{L} = \varphi_{CO_2}^{G} \rightarrow \frac{1}{K_{ov}} = \frac{1}{k_G} + \frac{1}{k'_{liq}} \tag{9}$$

where $\varphi_{CO_2}^{G}$ [mol/(s m^2)] is the CO_2 flux in the gas phase, k_G [mol/(m^2 s Pa)] is the gas-side mass transfer coefficient, $P_{CO_2}^{gas}$ [Pa] is the partial pressure of CO_2 in the gas bulk, $P_{CO_2}^{int}$ [Pa] is the partial pressure of CO_2 at the interface, $\varphi_{CO_2}^{L}$ [mol/(s m^2)] the CO_2 flux in the liquid phase, k_{liq} [m/s] is the liquid-side mass transfer coefficient based on the liquid concentrations, $C_{CO_2}^{int}$ [mol/m^3] is the CO_2 concentration in the liquid phase at the interface, $C_{CO_2}^{liq}$ [mol/m^3] is the concentration in the liquid bulk, k'_{liq} [mol/(m^2 s Pa)] is the liquid-side mass transfer coefficient based on partial pressures, $P_{CO_2}^{liq}$ [Pa] is the partial pressure of carbon dioxide in the liquid bulk, φ_{CO_2} [mol/(s m^2)] is the CO_2 flux, and K_{ov} [mol/(m^2 s Pa)] is the overall mass transfer coefficient.

The K_{ov} was measured for different solvent compositions and temperatures by changing the reaction temperature, the concentration of ammonia in the solvent, the concentration of K_2CO_3 in the solvent, and the CO_2 loading. Once the operation point was determined by setting these parameters, the CO_2 absorption was measured at five different CO_2 partial pressures in the reactor by changing the CO_2 composition in the gas phase. Matching the values of φ_{CO_2} and $P_{CO_2}^{gas}$ gives a chart like that shown in Figure 6, where the slope is represented by the K_{ov} and the intercept with the *x* axis is the $P_{CO_2}^{liq}$. The

approach used herein to measure the overall mass transfer coefficient neglects the ammonia slip in the reaction chamber. This assumption is supported by a simulation of the reaction chamber that was previously carried out with a rate-based approach in Aspen Plus with the Extended UNIQUAC thermodynamic model (Jayaweera and Jayaweera, 2018), the results of which estimated an ammonia loss of less than 3% of the total ammonia present in the solvent during the course of the experiment.

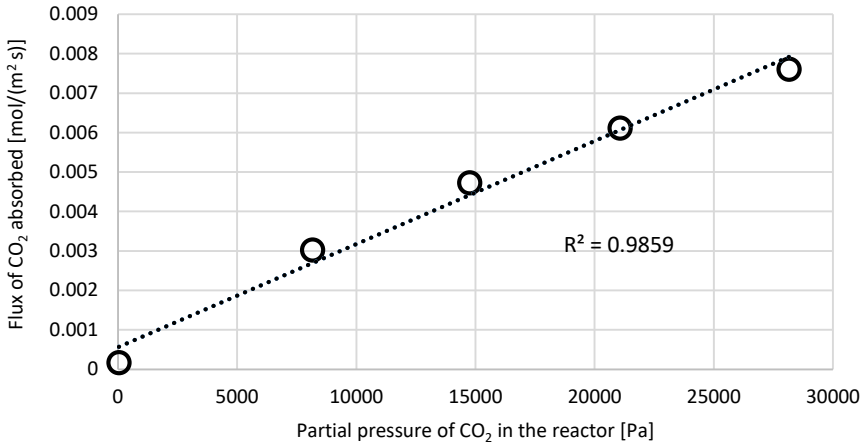

Figure 6. Flux of CO_2 absorbed as a function of CO_2 partial pressure in the reactor for the case with NH_3 molality of 2.5, K_2CO_3 molality of 1.5, CO_2 loading 0.35, and temperature of 25 °C. The overall mass transfer coefficient, K_{ov}, is the slope of the trend line, the intercept indicates the partial pressure of CO_2 in the liquid, and the R^2 is the correlation coefficient which determines the degree of agreement between the fitted line and the experimental data.

4. Results and discussion

The influences of K_2CO_3, NH_3, and temperature on the heat of desorption are discussed in the following sections. Variations in these parameters were very important for the heat duty during regeneration of the solvent. The impact of K_2CO_3 on the ammonia slip is also discussed. Ammonia slip is one of the main drawbacks associated with the use of ammonia-based solvents. Finally, the WWC results are presented and explained with the support of the Extended UNIQUAC thermodynamic model.

4.1. CO_2 absorption and CO_2 desorption properties of the Mixed-Salt Technology solvent

The capture of CO_2 by chemical absorption is based on the ability of the solvent to absorb CO_2 at low temperature and desorb CO_2 at high temperature. The absorption is exothermic, so the temperature of the solvent rises while absorbing CO_2. In the regeneration process, the solvent is heated to a temperature of around 120 °C. This causes the desorption of CO_2, an endothermic reaction. Solvent regeneration is the part of the process requiring the largest amount of energy, so the heat of CO_2 desorption is a key thermodynamic property for reducing the heat duty of this process.

The graphs in Figure 7 represent the heat duty for different mixes of NH_3 and K_2CO_3. The curves shown are iso-capacity curves. Iso-capacity is the sum of the molality of NH_3 and the molality of K_2CO_3, and is defined as:

$$iso\text{-}capacity = \frac{n_{NH_3} + n_{K_2CO_3}}{m_{H_2O}} \quad (10)$$

where n_{NH_3} is the amount of ammonia in the solvent [mol], $n_{K_2CO_3}$ is the amount of K_2CO_3 in the solvent [mol], and m_{H_2O} is the mass of water (the solvent) [kg_{H2O}]. The result is the sum of the molality of ammonia and the molality of potassium carbonate. The approach and the equations used for the computation of the heat of CO_2 desorption are described in the work by Darde et al. (2012).

The *x*-axis in the graphs indicates the molality of K_2CO_3 in the solvent. The molality of NH_3 can then be calculated using the iso-capacity of the specific curve. The *y*-axis represents the heat of CO_2 desorption, calculated considering a carbon capture of 90% from exhaust containing 13% CO_2 at 1 bar of pressure (which are the typical conditions for a coal power plant). Hence, the heat of desorption is calculated at a determined temperature for a solvent CO_2 loading corresponding to a partial pressure of CO_2 under lean conditions at 0.013 bar and 20 °C (the inlet temperature in the absorber).

The curves in the graphs are interrupted at the points where salt deposition takes place at the rich loading (a CO_2 partial pressure of 0.13 bar at 40 °C). Both graphs show data recorded at a constant regeneration temperature; the left-hand graph in Figure 7 at 120 °C and the right-hand graph at 130 °C.

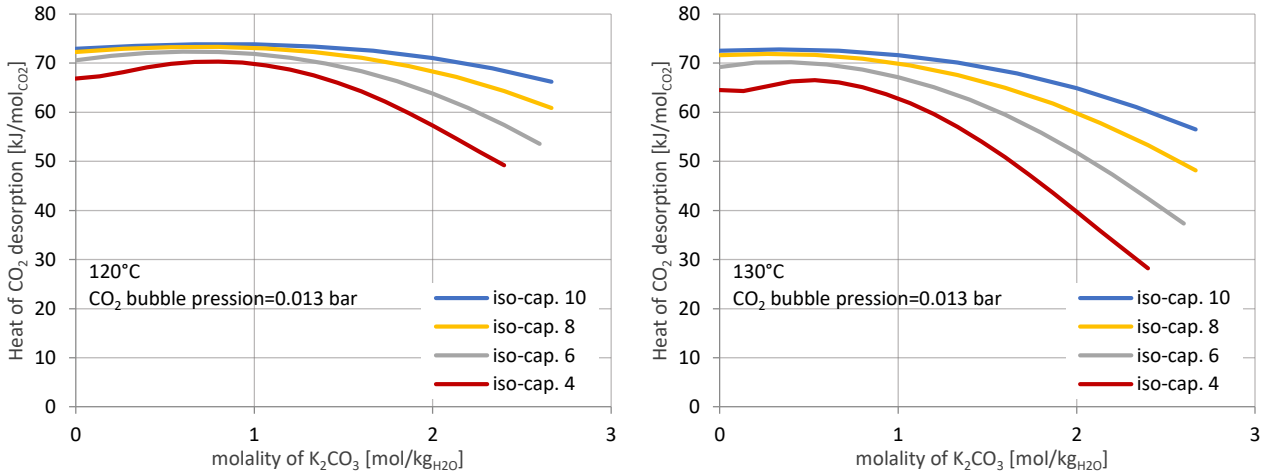

Figure 7. Heat of CO_2 desorption at 120 °C (left) and 130 °C (right) as a function of solvent composition at different iso-capacity values expressed as the definition given in (Eq. (10)) in [mol/kg_{H2O}]. The curves extend until the points at which salt deposition occurs.

The results indicate a benefit in terms of heat of desorption upon increasing the fraction of K_2CO_3 in the solvent, which agrees with the results of a previous study (Jayaweera et al., 2016). This impact was greater at increased regeneration temperatures, and reduced the iso-capacity of the solvent. Indeed, upon increasing the temperature, the molality of carbonate ions increased relative to that of bicarbonate ions, reducing the heat of desorption. Thus, increasing the amount of K_2CO_3 in the solvent amplified this effect. Moreover, at the same molality of potassium carbonate, the ratio of potassium ions to ammonium ions increased as the iso-capacity decreased, so the impact of the K_2CO_3 concentration on the heat of desorption was larger at lower iso-capacity. On the other hand, when the molality of K_2CO_3 was more than 2.5 mol/kg_{H2O}, the solution became supersaturated and salt deposition took place. The analysis identified the most desirable properties for the solvent with an iso-capacity of 4 mol/kg_{H2O}. In detail, the

heat of desorption increased until approximately 1 molal K_2CO_3 and then decreased upon increasing the K_2CO_3 molality further, as already mentioned. This phenomenon is explained by the speciation reported in Figure 8 for the cases of iso-capacity 4 and 8. Indeed, when the concentration of aqueous CO_2 in the solvent was low, the heat of desorption was mainly affected by the ion concentrations. On the other hand, when the concentration of aqueous CO_2 was high enough (above approximatively 1 molal K_2CO_3), the heat of desorption was not strictly dependent on the concentrations of ions in the solution, and the heat of desorption was lower.

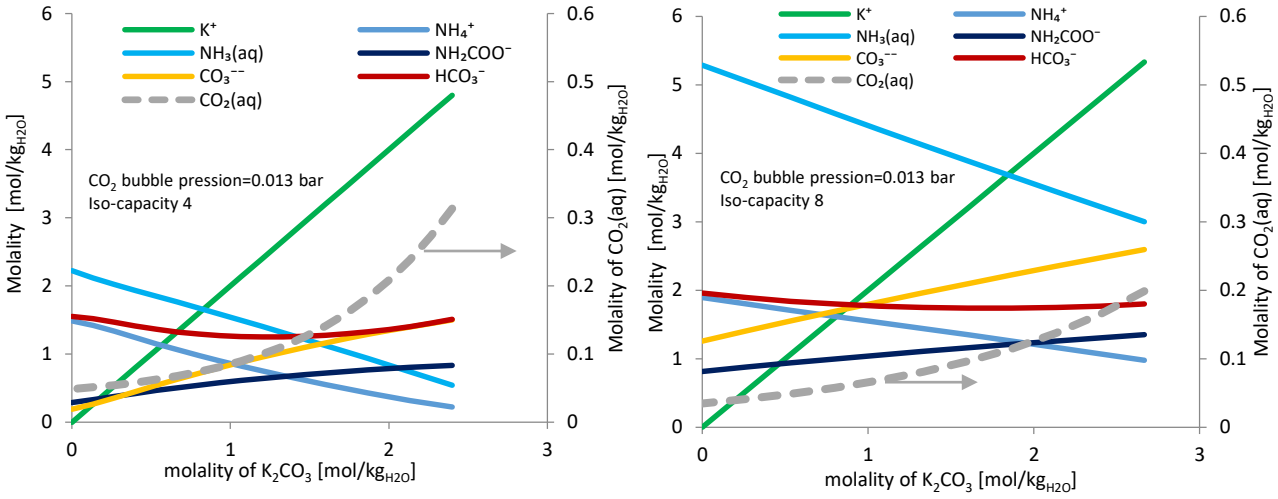

Figure 8. (Left) The molality of each species in liquid phase as a function of the molality of K_2CO_3, for the case with iso-capacity of 4. The solid lines correspond to the left *y*-axis, while the dashed grey line corresponds to the right *y*-axis. (Right) The molality of each species in liquid phase as a function of the molality of K_2CO_3, for the case with iso-capacity of 8. The solid lines correspond to the left *y*-axis, while the dashed grey line corresponds to the right *y*-axis.

Figure 9 highlights the impact of regeneration temperature on the heat of desorption in different mixtures of NH_3 and K_2CO_3 for an iso-capacity of 4 mol/kg_{H2O}. The results show that temperature exerts a weak influence on the heat of desorption of CO_2 from an aqueous ammonia solvent. When the K_2CO_3 fraction was increased, an increased regeneration temperature reduced the heat of desorption. This effect is due to the higher concentration of CO_3^{2-} due to dissociation of K_2CO_3. Increased CO_3^{2-} levels shifted the

equilibrium toward a higher concentration of $CO_{2(aq)}$, so the impact of CO_2 solubility, which decreases as the temperature increases, thereby reduces the heat of CO_2 desorption.

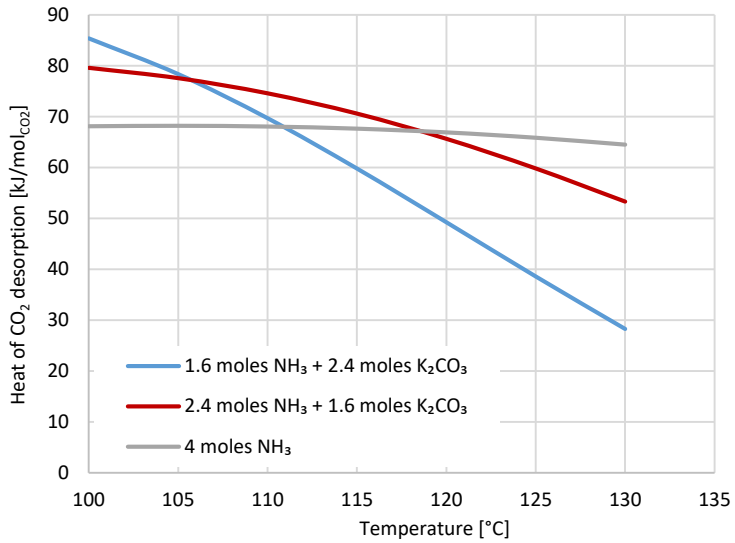

Figure 9. Temperature dependence of the heat of CO_2 desorption for different mixtures of H_2O-NH_3-K_2CO_3.

4.2. Ammonia slip of the Mixed-Salt Technology solvent

Ammonia slip is one of the main drawbacks of ammonia-based solvent technology. The addition of potassium carbonate to the solvent mixture changes the solubility of ammonia in the solvent and, consequently, its volatility. The parameter considered to best describe the ammonia slip is the partial pressure of ammonia. Indeed, at higher partial pressures of ammonia, the ammonia is more volatile and thus the slip in the absorption column is greater.

Figure 10 depicts the partial pressure of ammonia for different constant-capacity lines of the solvent. The points presented correspond to a constant CO_2 partial pressure (0.013 bar) and a temperature of 25 °C. The solid lines change to dashed lines at the points where salt precipitation begins. Figure 10 shows that the partial pressure of ammonia initially increased, but then decreased with increasing K_2CO_3 in the solvent. In consideration of the salt precipitation, the constant-capacity line with the greatest benefits in

terms of the range of its values is the line corresponding to 4 mol/kg_{H2O}. Similar behavior in this mixture was reported previously (Jayaweera et al., 2016), wherein a decreasing partial pressure of ammonia upon increasing the K_2CO_3 content in the Mixed-Salt solvent was reported.

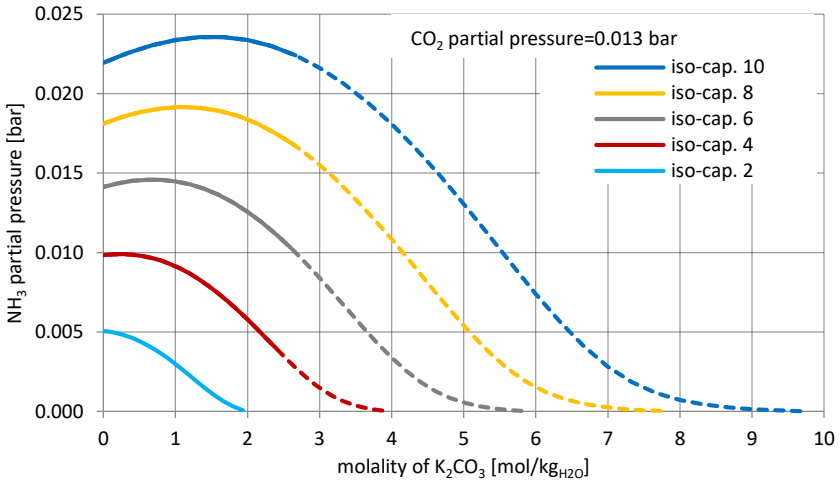

Figure 10. Partial pressure of ammonia as a function of initial K_2CO_3 molality for different iso-capacities of the solvent. The partial pressure of CO_2 was constant at 0.013 bar, and the temperature was 25 °C. The solid lines are the conditions prior to salt precipitation, while the dashed line represent the points where salt precipitation occurs.

Figure 11 (left) shows the partial pressure of ammonia at constant CO_2 partial pressure (0.013) and at varying initial ammonia concentration at 25 °C as a function of the K_2CO_3 content. Figure 11 (right) depicts the concentration of species for the solvent with an initial concentration of 4 molal ammonia as a function of the K_2CO_3 content in the solvent.

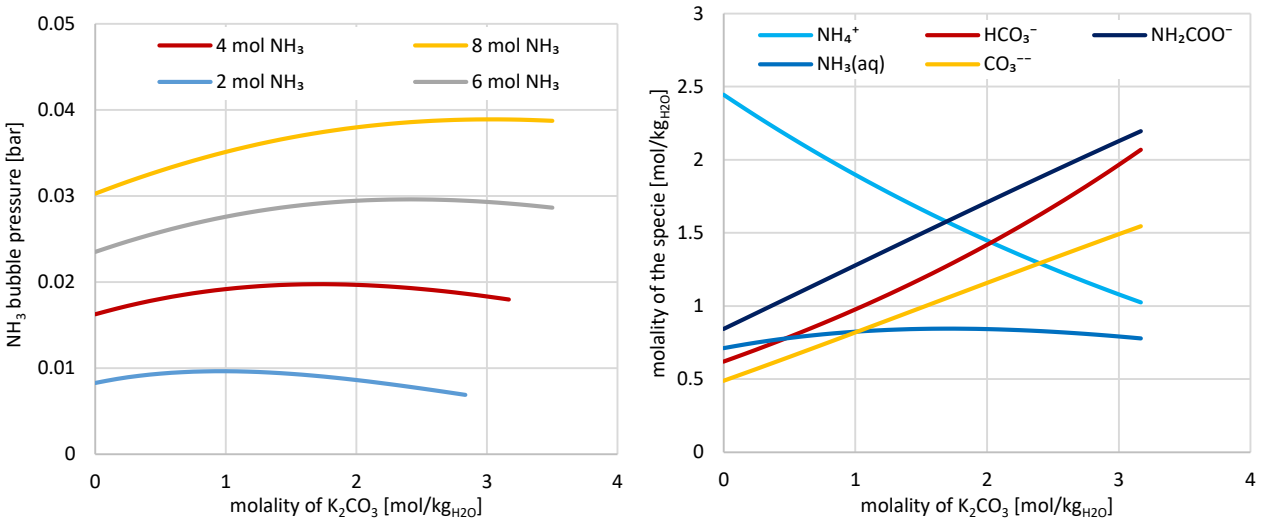

Figure 11. (Left) Ammonia partial pressure as a function of the K_2CO_3 concentration for different ammonia initial concentration. The partial pressure of CO_2 is constant, 0.013 bar, and the temperature is 25 °C. (Right) Molality of every species in the solvent for a solvent with an initial ammonia molality of 4. In both charts the lines are interrupted when salt precipitation starts.

The results do not indicate any significant variation in the partial pressure of ammonia with increasing fraction of K_2CO_3 in the solvent. Since K_2CO_3 is a weak base, at the beginning it shifts the reaction (R2) equilibrium toward an increased $NH_{3(aq)}$ concentration and reduced concentration of NH_4^+, with the effect of a weak increase in the ammonia slip. However, upon increasing the K_2CO_3 concentration further, the equilibrium of the reactions (R2) and (R5) maintain the $NH_{3(aq)}$ concentration stable, and the NH_4^+ reacts to form NH_2COO^-. This is a beneficial property of the solvent, since the ammonia slip remains constant while the higher concentration of K_2CO_3 increases the capacity of the solvent.

4.3. Overall mass transfer coefficient and kinetics of absorption

The property measured with the WWC is the overall mass transfer coefficient (K_{ov}), according to the definition in equation (8).

316 During the absorption of CO_2 by the aqueous ammonia and potassium carbonate solvent, three main
317 reactions occur in the liquid film and drive the kinetics of absorption. These reactions are the formation
318 of carbonic acid (R6), the formation of bicarbonate (R7), and the formation of carbamate (R8):

$$CO_{2(aq)} + H_2O \leftrightarrow HCO_3^- + H^+ \quad \text{(R6)}$$

$$CO_{2(aq)} + OH^- \leftrightarrow HCO_3^- \quad \text{(R7)}$$

$$CO_{2(aq)} + 2\,NH_3 \leftrightarrow NH_2COO^- + NH_4^+ \quad \text{(R8)}$$

319 According to Blauwhoff (1983), reaction (R6) has a negligible contribution to the overall rate of
320 absorption because this reaction is very slow compared to the others involved.

321 The rate of reaction (R7), $r_{CO_2-OH^-}$ [mol/(m^3 s)], was described previously in an experimental study by
322 Pinsent et al. (1956), which indicated second-order reaction kinetics in an Arrhenius expression of the
323 kinetic constant:

$$r_{CO_2-OH^-} = k_{OH^-} C_{CO_2} C_{OH^-} \quad with \quad k_{OH^-} = 4.2 * 10^{13}\, exp\left(\frac{-24069\ \left[\frac{J}{mol}\right]}{RT}\right) \quad (11)$$

324 where k_i [1/s] is the kinetic constant for the component i and C_i [mol/m^3] is the concentration of
325 component i.

326 The rate of reaction (R8) was described in an experimental study by Lillia et al. (2018a):

$$r_{CO_2-NH_3} = k_{NH_3} C_{CO_2} C_{NH_3}^{\gamma} \quad with \quad k_{NH_3} = 1.41 * 10^{8}\, exp\left(-\frac{60680\ \left[\frac{J}{mol}\right]}{RT}\right) and\ \gamma = 1.89 \quad (12)$$

327 where 60680 J/mol is the activation energy, 1.41×10^8 [m^3/(mol s)] is a pre-exponential factor of the
328 Arrhenius constant, and γ is an experimentally fitted coefficient.

329 Figure 12 reports the overall mass transfer coefficient (K_{ov}) of the solvent under 18 different conditions.
330 The *x*-axis represents the initial molality of K_2CO_3 in the solvent, while the *y*-axis represents the K_{ov}.

The solvent was analyzed for both lean and rich loadings at three different temperatures (25 °C, 35 °C, and 45 °C).

The CO_2 loading of the solvent is defined as:

$$CO_2\ load. = \frac{n_{app,CO_2} - n_{K_2CO_3}}{n_{NH_3} + n_{K_2CO_3}} \quad (13)$$

where n_{NH_3} is the initial amount of NH_3 in the solvent in moles, $n_{K_2CO_3}$ is the initial amount of K_2CO_3 in the solvent in moles, and n_{app,CO_2} is the apparent amount of CO_2 in moles. The numerator is determined by the difference between the apparent amount of CO_2 and amount of K_2CO_3 because it considers only the additional CO_2 absorbed without considering the CO_2 available in K_2CO_3.

The experimental analysis focused on the iso-capacity of 4 mol/kg_{H2O} since it was the most promising with respect to its thermodynamic properties and salt deposition behavior. Moreover, the iso-capacity of 4 mol/$_{kgH2O}$ maintains a high regeneration pressure in every solvent composition since the bubble pressure of CO_2 at 120 °C is always higher than 10 bar at a lean CO_2 loading, which allows a CO_2 capture of 90% in a typical coal plant. The three solvent compositions analyzed were 4 molal NH_3 without K_2CO_3, 2.5 molal NH_3 with 1.5 molal K_2CO_3, and 1.5 molal NH_3 with 2.5 molal K_2CO_3.

The lean loading was 0.35 for the case of 4 molal NH_3 and 0.25 for the other two cases containing K_2CO_3. These values were chosen in consideration of a partial pressure of CO_2 of less than 0.013 bar (specifically, 0.003 bar) which comprises a driving force to achieve capture of 90% of CO_2 from the flue gas of a coal-fired power plant. The same logic was adopted to estimate the rich loadings of 0.45 for the case of 4 molal NH_3 and of 0.35 for the other two solvent mixtures. In this way, a comparison between the kinetic conditions possible at the top and bottom of an absorption column with different solvent mixtures could be assessed. These loading values were not taken from a pilot plant, so they are not an index of the cyclic capacity of the solvent since they are not correlated. The lean and rich loading values were taken in order

to highlight the effect of the loading on the overall mass transfer coefficient, based on two different loadings that could be used in a capture plant.

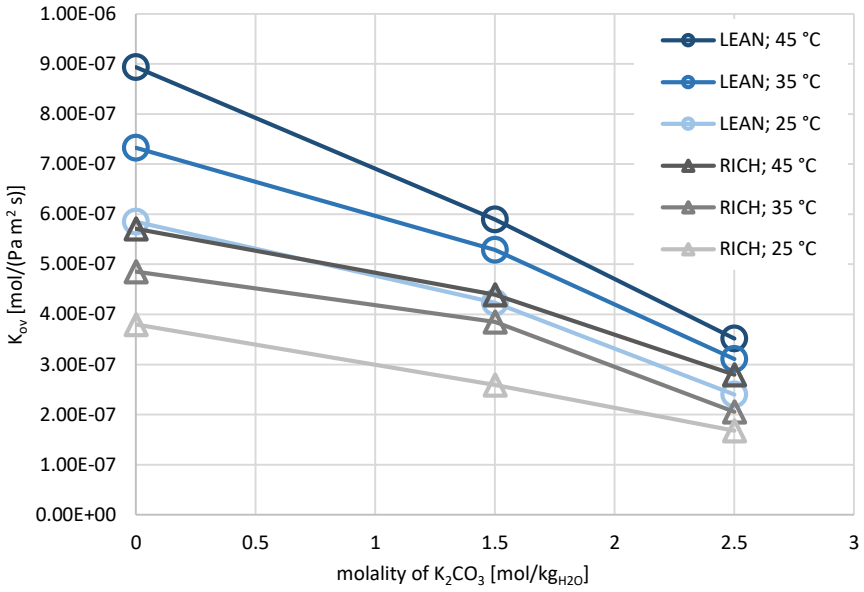

Figure 12. Overall mass transfer coefficient, K_{ov}, as a function of K_2CO_3 molality for solvents with iso-capacity of 4 mol/kg_{H2O}. The data were measured at 3 different temperatures (25 °C, 35 °C, and 45 °C) and 2 different CO_2 loadings (lean and rich).

The first trend analyzed from the results shown in Figure 12 was the dependence of K_{ov} on the CO_2 loading. The results show that K_{ov} decreased with increased CO_2 loading of the solvent. Indeed, the solvents with rich loadings were more saturated by CO_2, and consequently the reactant concentrations in the liquid phase were lower since they had already reacted with the CO_2. As shown by equations (6) and (12), the rates of reactions (R7) and (R8) are dependent on the reactant concentrations, which were reduced in this case due to reactions with the loaded CO_2.

The second trend analyzed was the temperature dependence; the results confirm the Arrhenius expression of the kinetic constant shown in equation (11). As indicated in equation (12), there is an exponential dependence of K_{ov} on temperature following the Maxwell-Boltzmann distribution of the kinetic energy of the molecules, where increasing the temperature of the reaction increases the rate of reaction.

The third trend analyzed was the effect of different proportions of NH_3 and K_2CO_3 at constant iso-capacity on the K_{ov}. The results indicated a reduction in the K_{ov} with increasing fraction of K_2CO_3 in the solvent. Indeed, as demonstrated in Figure 13, with increasing K_2CO_3 content, the free ammonia, $NH_{3(aq)}$, in the liquid decreased. As demonstrated by Darde et al.(2011) and Lillia et al. (2018a), among the reactions (R6) to (R8), reaction (R8) contributes most significantly to the overall kinetics of absorption. This explains why the K_{ov} decreased with decreasing free ammonia concentration in the liquid, where reaction (R8) involves high concentrations of reagents and contributes significantly to the rate of absorption. On the other hand, the impact of free ammonia concentration becomes less significant as the K_2CO_3 concentration increases, at which point the influence of reaction (R8) on the rate of absorption decreases and the contribution by reaction (R6) increases.

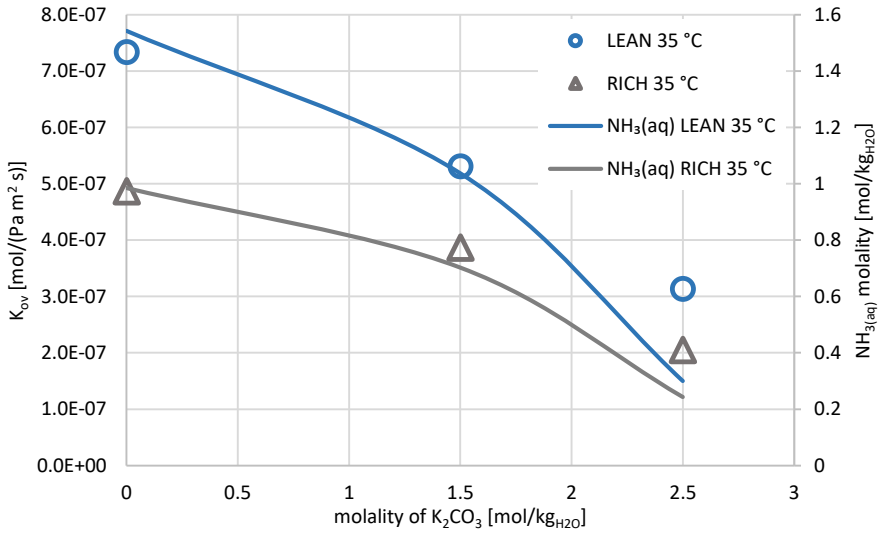

Figure 13. The overall mass transfer coefficient is represented as a function of the initial molality of K_2CO_3 (left *y*-axis); the blue circles represent the values at 35 °C and lean loadings while the grey triangles represent the values at 35 °C and rich loadings. The molality of free ammonia ($NH_{3(aq)}$) in the solvent is represented as a function of the initial molality of K_2CO_3 (right *y*-axis); the blue solid line represents the values at 35 °C and lean loadings while the grey solid line represents the values at 35 °C and rich loadings.

For the sake of completeness, Figure 14 reports the speciation as a function of the CO_2 loading at 35 °C for three different mixtures of NH_3 and K_2CO_3. Since there is a correlation between reactant concentration in the liquid and the reaction kinetics, the speciation, especially the concentration of $NH_{3(aq)}$, can be used to predict trends in K_{ov} and consequently in the kinetics of absorption.

As shown in all three graphs of Figure 14, the $NH_{3(aq)}$ concentration decreased with increasing CO_2 loading. It follows that the K_{ov} would decrease with increased CO_2 loading, which was confirmed by the experiment and explained previously. When the CO_2 loading increased, the concentration of NH_2COO^- also increased, up to a CO_2 loading of about 0.5, and thus carbamate is the main species formed by CO_2. Beyond this loading, the concentration of HCO_3^- increased, finally exceeding the concentration of NH_2COO^-. At the same time, free ammonia forms NH_4^+ as pH decreases due to CO_2 absorption. The ammonium cation then combines with bicarbonate to form ammonium bicarbonate (NH_4HCO_3), which is the main ammonium salt formed in the carbon capture process.

Comparing the results of the three graphs of Figure 14 corresponding to the different mixtures of NH_3 and K_2CO_3, it can be concluded that reducing the NH_3 concentration resulted in a decrease in the concentration of free ammonia. Consequently, the rate of absorption decreased, as supported by the results shown in Figure 13. Further, increasing the K_2CO_3 concentration in the solvent resulted in a higher concentration carbonate ions (CO_3^{2-}). The presence of carbonate ions and potassium ions (K^+) changes the equilibrium of the bicarbonate ions when the CO_2 loading increases. Indeed, as shown by Figure 14, in the presence of K_2CO_3, the concentration of bicarbonate ions was higher in the solvents with higher CO_2 loadings. The same influence was also seen for the carbamate ion (NH_2COO^-), the concentration of which increased in the presence of K_2CO_3 in the solvent.

A further observation about the properties of the three different mixtures presented in Figure 14 concerns the carrying capacity of the solvent. The carrying capacity is defined as:

$$CC = \frac{m_{CO_2,app}}{V_{H_2O}} \left[\frac{g_{CO_2}}{L_{H_2O}}\right] \quad (14)$$

where CC is the carrying capacity [g_{CO2}/L_{H2O}], $m_{CO_2,app}$ is the apparent mass of CO_2 in the solvent [g_{CO2}], and V_{H_2O} is the volume of water in the solvent [L_{H2O}]. The carrying capacity indicates the capacity of one liter of solvent to dissolve and carry CO_2 in the liquid phase. Its value, calculated at 35 °C for the maximum loading before the saturation point, is 158.44 [g_{CO2}/L_{H2O}] for the solvent with 4 molal NH_3, 224.45 [g_{CO2}/L_{H2O}] for the solvents with 2.5 molal NH_3 and 1.5 molal K_2CO_3, and 233.25 [g_{CO2}/L_{H2O}] for the solvent with 1.5 molal NH_3 and 2.5 molal K_2CO_3. Thus, increasing the fraction of K_2CO_3 in the solvent resulted in increased carrying capacity.

Finally, Figure 15 shows the K_{ov} for the aqueous ammonia solvent and MEA solvent at different concentrations, different CO_2 loadings, and different temperatures, in order to allow for qualitative comparisons with the Mixed-Salt solvent. The order of magnitude of the values of K_{ov} for the Mixed-Salt solvent compositions analyzed herein is the same as that of the values reported for the NH_3 and MEA solvents, as shown in Figure 15. Considering the temperature range and the loading of the Mixed-Salt solvent analyzed, the values of K_{ov} for the ammonia and MEA shown in Figure 15 are on average 1.5-2 times larger (4e-7÷1.4e-6 mol/(Pa m^2 s)) than those of the Mixed-salt solvent (ranging from 2e-7÷8e-7 mol/(Pa m^2 s)), and by extension the size of the absorber required would be expected to be 1.5-2 times larger. However, the K_{ov} depends on the concentration of the reagent in the solvent, and the iso-capacity 4 was selected based on thermodynamic properties. Increasing the iso-capacity also increased the K_{ov}, reducing the size of the absorber needed but hurting the performance of the process in terms of energy efficiency. Moreover, the reduction in the ammonia slip in the Mixed-Salt solvent might allow higher temperatures to be used in the absorber, increasing the K_{ov} process.

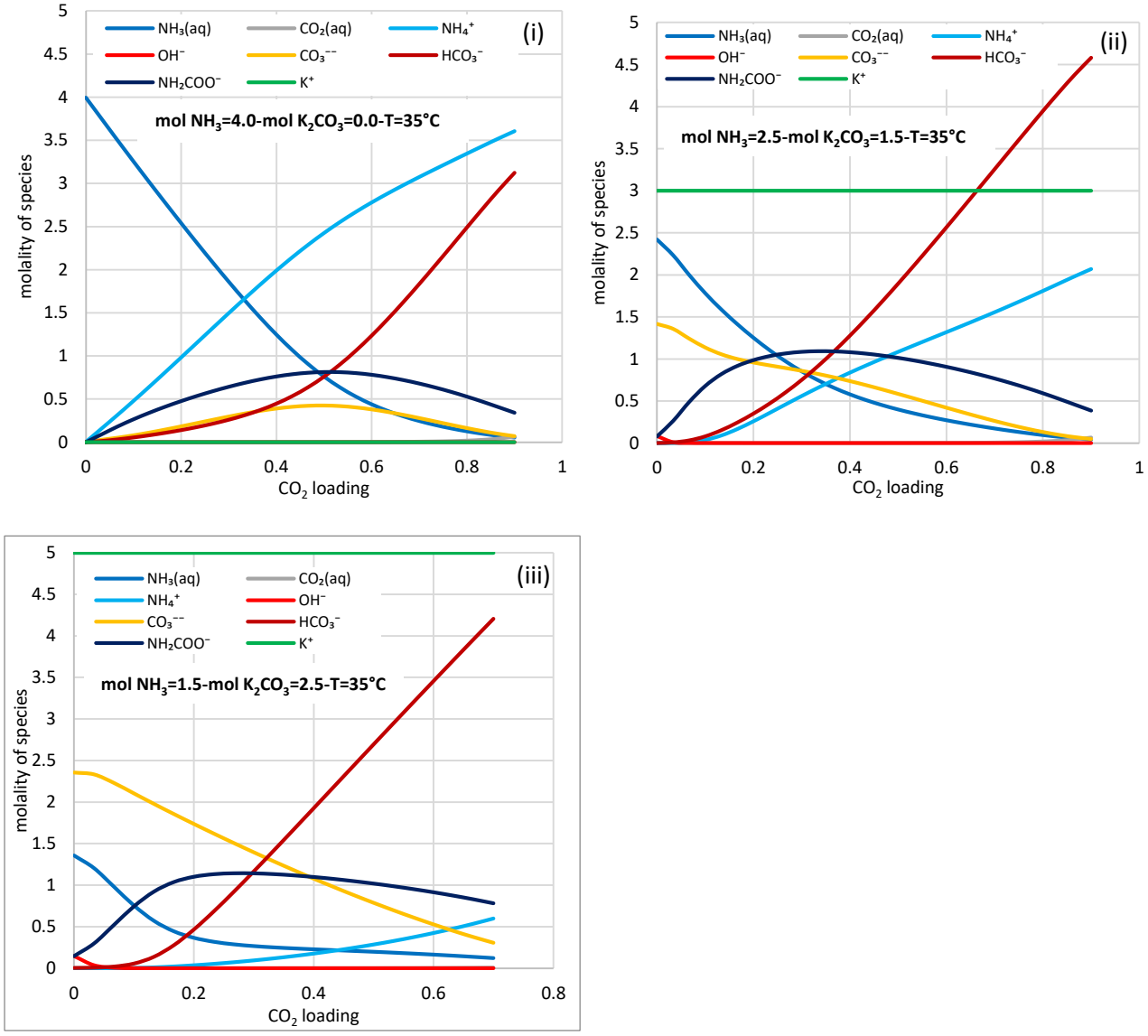

Figure 14. The graphs represent the molality of the different species in the liquid phase as a function of CO_2 loading at 35 °C for (i) the solvent with NH_3 molality of 4, (ii) the solvent with NH_3 molality of 2.5 and K_2CO_3 molality of 1.5, and (iii) the solvent with NH_3 molality of 1.5 and K_2CO_3 molality of 2.5.

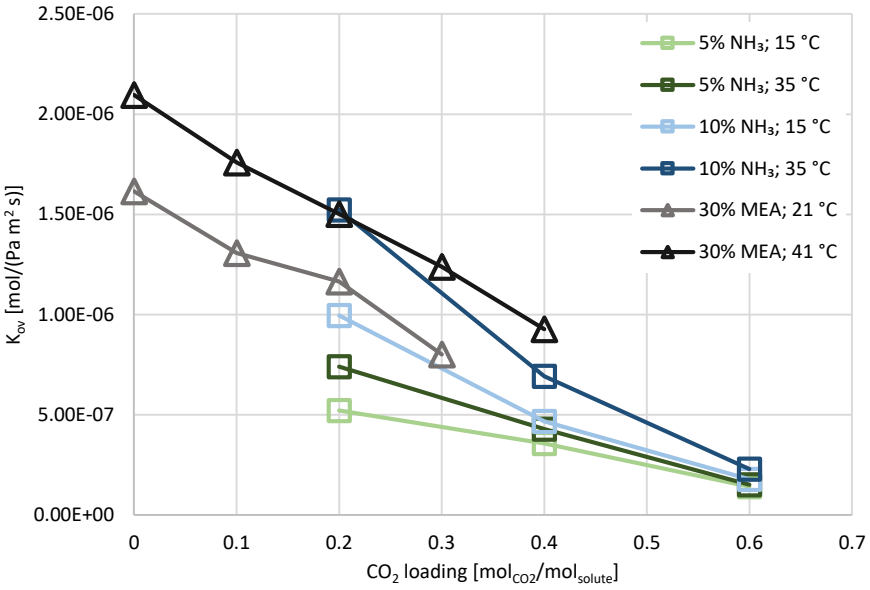

Figure 15. Overall mass transfer coefficient, K_{ov}, as a function of the CO_2 loading at different solvent concentrations and different temperatures. The experimental data for the MEA solvent was taken from the work by Darde et al. (2011), while the data for the NH_3 solvent was taken from the work by Lillia et al. (2018a).

5. Conclusions

This work presented the thermodynamic and kinetic properties of CO_2 absorption in the NH_3-K_2CO_3-CO_2-H_2O solvent system. The thermodynamic properties and the speciation of the solvent were calculated with the Extended UNIQUAC thermodynamic model, while the kinetics of absorption were measured experimentally using a WWC setup.

The heat of desorption decreased with increased regeneration temperature. For instance, heat of desorption of the solvent comprised of 2 molal NH_3 and 2 molal K_2CO_3 decreased from 58 kJ/mol_{CO2} at 120 °C to 40 kJ/mol_{CO2} at 130 °C. The heat of desorption also decreased when the fraction of K_2CO_3 in the solvent was increased, and this effect overshadowed the effect of increasing the regeneration temperature. For instance, at 120 °C, the heat of desorption decreased from 70 kJ/mol_{CO2} (for a mixture

of 3 molal NH_3 and 1 molal K_2CO_3) to 55 kJ/mol_{CO2} (for a mixture of 2 molal NH_3 and 2 molal K_2CO_3). The ammonia slip decreased with increasing fraction of K_2CO_3 in the solvent due to the decrease of free ammonia in the liquid phase. Increasing the concentration of K_2CO_3 in the solvent resulted in reduced solubility. Consequently, salt precipitation occurred at a lower CO_2 loading. The overall mass transfer coefficient increased with increasing temperature and decreased with increasing CO_2 loading, following the kinetic description of the Arrhenius equation.

The overall mass transfer coefficient decreased with increased fraction of K_2CO_3 in the solvent due to the reduction in the amount of free ammonia in the reactive layer. For instance, between the solution of 4 molal NH_3 and the solution of 1.5 molal NH_3 and 2.5 molal K_2CO_3 (both at 35 °C), the overall mass transfer coefficient decreased from 7.34×10^{-7} [mol/(Pa m^2 s)] to 3.14×10^{-7} [mol/(Pa m^2 s)].

The kinetics of absorption were mainly influenced by the reaction between free ammonia and CO_2. The overall mass transfer coefficient decreased with increasing K_2CO_3 fraction in the solvent.

The carrying capacity increased with increasing fraction of K_2CO_3 in the solvent, from 158.44 [g_{CO2}/L_{H2O}] for the solvent with 4 molal NH_3 to 224.45 [g_{CO2}/L_{H2O}] for the solvent with 1.5 molal NH_3 and 2.5 molal K_2CO_3.

The Mixed-Salt solvent had an overall mass transfer coefficient 1.5-2 times smaller than that of MEA.

Globally, the solvent has interesting properties for CO_2 capture applications. As a first analysis, the solvent compositions considered in this evaluation have good thermodynamic properties (low ammonia slip and low heat of desorption), with the drawback of slower absorption kinetics compared to those in an aqueous ammonia solvent.

Nomenclature:

Acronyms	
Bulk	Bulk layer
LCA	Life cycle assessment
WWC	Wetted wall column
WWC, in	Wetted wall column inlet
WWC, out	Wetted wall column outlet
Symbols	
A	pre-exponential factor of the Arrhenius constant [m^3/(mol s)]
A_{int}	interfacial area in the wetted wall column [m^2]
C_i^j	concentration of component i at position j [mol/m^3]
CC	carrying capacity [g_{CO2}/L_{H2O}]
H_{CO_2}	partition coefficient of CO_2 [(Pa m^3)/mol]
K_{ov}	overall mass transfer coefficient for the CO_2 transport [mol/(Pa m^2 s)]
k_i	kinetic constant for component i [m^3/(mol s)]
k_G	gas-side mass transfer coefficient [mol/(Pa m^2 s)]
k_{liq}	liquid-side mass transfer coefficient related to the difference in concentrations [m/s]
k'_{liq}	liquid-side mass transfer coefficient of the difference in partial pressure [mol/(Pa m^2 s)]
$m_{CO_2,app}$	apparent mass of CO_2 in the solvent [g_{CO2}]
N_i^j	molar flow of component i at position j [mol/s]
P_i^j	partial pressure of component i at position j [mol/s]
r_{i-j}	rate of reaction between components i and j [mol/(m^3 s)]
V_{H_2O}	volume of H_2O in the solvent [L_{H2O}]
y_i^j	mole fraction of component i at position j in the gas phase [-]
Greek symbols	
Δx	difference between the inlet and the outlet of the x variable
γ	experimental parameter [-]
φ_i^j	molar surface flow of species i in media j [mol/(m^2 s)]

Bibliography

Bai, H., Yeh, A.C., 1997. Removal of CO_2 Greenhouse Gas by Ammonia Scrubbing. Ind. Eng. Chem. Res. 36, 2490–2493. https://doi.org/10.1021/ie960748j

Blauwhoff, P.M.M., 1983. a Study on the Reaction Between CO_2 and Alkalonamines in aqueous solutions. Chem. Eng. Sci. 38, 1411–1429. https://doi.org/10.1016/0009-2509(83)80077-3

Bonalumi, D., Valenti, G., Lillia, S., Fosbøl, P.L., Thomsen, K., 2016. A Layout for the Carbon Capture with Aqueous Ammonia without Salt Precipitation. Energy Procedia 86, 134–143. https://doi.org/10.1016/j.egypro.2016.01.014

Cacciola, G., Restuccia, G., Aristov, Y., 1995. Vapor Pressure of (Potassium Hydroxide + Ammonia + Water) Solutions. J. Chem. Eng. Data 40, 267–270. https://doi.org/10.1021/je00017a058

Darde, V., Thomsen, K., van Well, W.J.M., Bonalumi, D., Valenti, G., Macchi, E., 2012. Comparison of two electrolyte models for the carbon capture with aqueous ammonia. Int. J. Greenh. Gas Control 8, 61–72. https://doi.org/10.1016/j.ijggc.2012.02.002

Darde, V., van Well, W.J.M., Fosboel, P.L., Stenby, E.H., Thomsen, K., 2011. Experimental measurement and modeling of the rate of absorption of carbon dioxide by aqueous ammonia. Int. J. Greenh. Gas Control 5, 1149–1162. https://doi.org/10.1016/j.ijggc.2011.07.008

Gladis, A., Gundersen, M.T., Fosbøl, P.L., Woodley, J.M., von Solms, N., 2017. Influence of temperature and solvent concentration on the kinetics of the enzyme carbonic anhydrase in carbon capture technology. Chem. Eng. J. 309, 772–786. https://doi.org/10.1016/j.cej.2016.10.056

Grant, T., Anderson, C., Hooper, B., 2014. Comparative life cycle assessment of potassium carbonate and monoethanolamine solvents for CO_2 capture from post combustion flue gases. Int. J. Greenh. Gas Control 28, 35–44. https://doi.org/10.1016/j.ijggc.2014.06.020

Hill, A.E., 1930. Hydrated Potassium Sesquicarbonate $K_2CO_3 \cdot 2KHCO_3 \cdot 3/2H_2O$. J. Am. Chem. Soc. 52, 3817–2825.

Jayaweera, I., Jayaweera, P., 2018. Development of Mixed-Salt Technology for Carbon Dioxide Capture from Coal Power Plants. https://doi.org/10.2172/1441205

Jayaweera, I., Jayaweera, P., Elmore, R., Bao, J., Bhamidi, S., 2014. Update on mixed-salt technology development for CO_2 capture from post-combustion power stations. Energy Procedia 63, 640–650. https://doi.org/10.1016/j.egypro.2014.11.070

Jayaweera, I., Jayaweera, P., Kundu, P., Anderko, A., Thomsen, K., Valenti, G., Bonalumi, D., Lillia, S., 2017. Results from Process Modeling of the Mixed-salt Technology for CO_2Capture from Post-combustion-related Applications, in: Energy Procedia.

https://doi.org/10.1016/j.egypro.2017.03.1220
Jayaweera, I., Jayaweera, P., Yamasaki, Y., Elmore, R., 2016. Mixed salt solutions for CO_2 capture, Absorption-Based Post-Combustion Capture of Carbon Dioxide. https://doi.org/10.1016/B978-0-08-100514-9.00008-1
Kamps, A.P.S., Meyer, E., Rumpf, B., Maurer, G., 2007. Solubility of CO_2 in aqueous solutions of KC1 and in aqueous solutions of K2CO3. J. Chem. Eng. Data 52, 817–832. https://doi.org/10.1021/je060430q
Kong, S., Application, F., Data, P., 2011. (12) United States Patent 2, 12–15. https://doi.org/10.1016/j.(73)
Lewis, W.K., Whitman, W.G., 1924. Absorption symposium. Ind. Eng. Chemnisty 16, 1215–1220. https://doi.org/10.1021/ie50180a002
Lillia, S., Bonalumi, D., Fosbøl, P.L., Thomsen, K., Valenti, G., 2018. Experimental study of the aqueous CO_2-NH_3 rate of reaction for temperatures from 15 °C to 35 °C, NH_3concentrations from 5% to 15% and CO_2 loadings from 0.2 to 0.6. Int. J. Greenh. Gas Control 70, 117–127. https://doi.org/10.1016/j.ijggc.2018.01.009
Lillia, S., Bonalumi, D., Fosbøl, P.L., Thomsen, K., Valenti, G., 2018. Experimental data of the aqueous NH_3 and CO_2 absorption at temperatures from 15 °C to 35 °C, NH_3 concentrations from 5% to 15% and CO_2 loadings from 0.2 to 0.6 measured with the Wetted Wall Column. Data Br. 17. https://doi.org/10.1016/j.dib.2018.02.047
Luzhnaya, N.P., Kosyachkova, S.N., 1955. Solubility isotherm at 50° of the quaternary system K2CO3-K2SO4-KHCO3-H2O.
Mumford, K.A., Smith, K.H., Anderson, C.J., Shen, S., Tao, W., Suryaputradinata, Y.A., Quyn, D.M., Qader, A., Hooper, B., Innocenzi, R.A., Kentish, S.E., Stevens, G.W., 2012. Erratum: Post-combustion capture of CO_2: Results from the Solvent absorption capture plant at hazelwood power station using potassium carbonate solvent (Energy and Fuels (2012) 26:1 (138-146) DOI: 10.1021/ef201192n). Energy and Fuels 26, 6449. https://doi.org/10.1021/ef3015519
Petrescu, L., Bonalumi, D., Valenti, G., Cormos, A.M., Cormos, C.C., 2017. Life Cycle Assessment for supercritical pulverized coal power plants with post-combustion carbon capture and storage. J. Clean. Prod. 157, 10–21. https://doi.org/10.1016/j.jclepro.2017.03.225
Pinsent, B.R.W., Pearson, L., Roughton, F.J.W., 1956. The kinetics of combination of carbon dioxide with hydroxide ions. Trans. Faraday Soc. 52, 1512. https://doi.org/10.1039/tf9565201512
Rochelle, G., Chen, E., Freeman, S., Van Wagener, D., Xu, Q., Voice, A., 2011. Aqueous piperazine as

the new standard for CO_2 capture technology. Chem. Eng. J. 171, 725–733. https://doi.org/10.1016/j.cej.2011.02.011

Rochelle, G.T.., 2011. Amine Scrubbing for CO_2 Capture. Science (80-.). 325, 19–22. https://doi.org/10.1126/science.1176731

Sorina, G.A., Miniovich, V.M., Efremova, G.D., 1967. Solubility of ammonia in aqueous solutions of KOH. Zhurnal Obs. Khimii 37, 2150–2154.

Thomsen, K., Rasmussen, P., 1999. Modeling of vapor–liquid–solid equilibrium in gas–aqueous electrolyte systems. Chem. Eng. Sci. 54, 1787–1802. https://doi.org/10.1016/S0009-2509(99)00019-6

Tosh, J.S., Field, J.H., Benson, H.E., Haynes, W.P., 1959. Equilibrium study of the system potassium carbonate, potassium bicarbonate, carbon dioxide, and water.

Trypuć, M., Kiełkowska, U., 1996. Solubility in the NH_4HCO_3 + NH_4VO_3 + H_2O System. J. Chem. Eng. Data 41, 1005–1007. https://doi.org/10.1021/je950290c

Williamson, R. V., Matheus, J.H., 1924. Endowment Fund. Ind. Eng. Chem. 16, 1102–1104. https://doi.org/10.1021/ie50179a001